Virus Research 167 (2012) 322–328

Contents lists available at SciVerse ScienceDirect

Virus Research

journal homepage: www.elsevier.com/locate/virusres

Short peptides derived from the interaction domain of SARS coronavirus nonstructural protein nsp10 can suppress the 2′-O-methyltransferase activity of nsp10/nsp16 complex

Min Ke[1], Yu Chen[1], Andong Wu, Ying Sun, Ceyang Su, Hao Wu, Xu Jin, Jiali Tao, Yi Wang, Xiao Ma, Ji-An Pan[2], Deyin Guo*

State Key Laboratory of Virology and Modern Virology Research Center, College of Life Sciences, Wuhan University, Wuhan 430072, People's Republic of China

ARTICLE INFO

Article history:
Received 2 April 2012
Received in revised form 20 May 2012
Accepted 22 May 2012
Available online 29 May 2012

Keywords:
SARS
Coronavirus
nsp10
nsp16
2′-O-methyltransferase
Peptides

ABSTRACT

Coronaviruses are the etiological agents of respiratory and enteric diseases in humans and livestock, exemplified by the life-threatening severe acute respiratory syndrome (SARS) caused by SARS coronavirus (SARS-CoV). However, effective means for combating coronaviruses are still lacking. The interaction between nonstructural protein (nsp) 10 and nsp16 has been demonstrated and the crystal structure of SARS-CoV nsp16/10 complex has been revealed. As nsp10 acts as an essential trigger to activate the 2′-O-methyltransferase activity of nsp16, short peptides derived from nsp10 may have inhibitory effect on viral 2′-O-methyltransferase activity. In this study, we revealed that the domain of aa 65–107 of nsp10 was sufficient for its interaction with nsp16 and the region of aa 42–120 in nsp10, which is larger than the interaction domain, was needed for stimulating the nsp16 2′-O-methyltransferase activity. We further showed that two short peptides derived from the interaction domain of nsp10 could inhibit the 2′-O-methyltransferase activity of SARS-CoV nsp16/10 complex, thus providing a novel strategy and proof-of-principle study for developing peptide inhibitors against SARS-CoV.

© 2012 Elsevier B.V. All rights reserved.

1. Introduction

Coronaviruses are the largest RNA viruses, which are enveloped and contain a single-stranded, positive-sense RNA genome ranging from 27 to 31.5 kb in length. They have long been recognized as pathogens of humans and animals such as feline, bovine, mouse and swine. The genome of severe acute respiratory syndrome coronavirus (SARS-CoV) is ~29.7 kb long and contains 14 open reading frames (ORFs) flanked by 5′ and 3′-untranslated regions of 265 and 342 nucleotides in length, respectively (Snijder et al., 2003). The 5′-proximal two third of the genome encodes 2 large overlapping ORFs (1a and 1b), which encode the proteins making the replication and transcription complex (RTC). While ORF1a is translated from the genome RNA to produce the polyprotein 1a, ORF1b is expressed by a −1 ribosomal frameshifting at the end of ORF1a to generate a large polyprotein (pp1ab) covering both ORF1a and 1b (Dos Ramos et al., 2004). These two polyproteins are cleaved into 16 mature replicase proteins, named as nonstructural proteins nsp1-16, which assemble the RTC located on a dedicated membrane surface (van Hemert et al., 2008). Of the 16 nsps, nsp14 was shown as exoribonuclease and (guanine-N7)-methyltransferase (N7-MTase) (Chen et al., 2007, 2009; Minskaia et al., 2006) and nsp16 as a 2′-O-methyltransferase (2′-O-MTase) (Chen et al., 2011; Decroly et al., 2008).

In previous studies, we and others have performed screenings to explore the interactions between SARS-CoV-encoded proteins by yeast two-hybrid (Y2H) or mammalian two-hybrid (M2H) systems (Imbert et al., 2008; Pan et al., 2008; von Brunn et al., 2007). It was demonstrated that nsp10 of SARS-CoV could interact with nsp14 and nsp16, respectively (Pan et al., 2008; von Brunn et al., 2007). The crystal structure revealed that nsp10 belongs to a new class of zinc finger proteins and was proposed to be a viral transcription factor (Joseph et al., 2006; Su et al., 2006). It was also shown that SARS-CoV nsp16 acts as a 2′-O-MTase in complex with nsp10 to selectively 2′-O-methylate the cap-0 structure to cap-1 structure (m7GpppAm-RNA) (Bouvet et al., 2010; Chen et al., 2011). Recently, we and Bruno Canard's group independently resolved the crystal structure of nsp10/nsp16 complex (Chen et al., 2011; Debarnot et al., 2011). We further demonstrated that nsp10 acts as the active partner of nsp16 by stabilizing the SAM-binding pocket and extending the substrate RNA-binding groove of nsp16 (Chen et al., 2011;

Abbreviations: SARS-CoV, severe acute respiratory syndrome coronavirus; nsp, nonstructural protein; RTC, replication and transcription complex; aa, amino acid.

* Corresponding author. Tel.: +86 27 68752506.
E-mail address: dguo@whu.edu.cn (D. Guo).
[1] These authors contributed equally to this work.
[2] The author is currently working at Department of Molecular Genetics and Microbiology, Stony Brook University, USA.

0168-1702/$ – see front matter © 2012 Elsevier B.V. All rights reserved.
http://dx.doi.org/10.1016/j.virusres.2012.05.017

Debarnot et al., 2011). Also it was reported that 2′-O-methylation of viral mRNA cap provides a molecular signature for the distinction of self and non-self mRNA, indicating that nsp16 may help the virus to evade host innate immunity (Daffis et al., 2010; Zust et al., 2011). Altogether, nsp16 plays a key role in the life-cycle of coronaviruses and the interaction between nsp10 and nsp16 is crucial for the functions of nsp16. Thus, inhibition of viral MTase activity should be able to suppress viral replication and attenuate viral virulence in infection and pathogenesis. The MTase active site was suggested as a drug target for developing antiviral drugs (Dong et al., 2008; Moheshwarnath Issur, 2011; Shuman, 2001). However, the MTase fold is structurally conserved between viral and cellular MTases, and it is thus difficult to obtain antiviral compounds with high specificity targeting MTase active sites. For this reason, it looks more promising to target the interface of nsp16 and nsp10 complex, which is unique to coronaviruses (Chen et al., 2011).

Although the crystal structure of nsp10/nsp16 complex is available, it is of importance to map the minimal domain of SARS-CoV nsp10 needed for its interaction with nsp16 and define the functional domain of nsp10 that is essential for stimulating nsp16 MTase activity. Such knowledge would be useful for designing and developing small molecules as protein–protein interaction inhibitors that could specially inhibit the enzymatic activity of nsp16 and the replication of SARS-CoV. Lugari and colleagues identified a number of key nsp10 residues involved in the interaction with nsp16 and in regulating nsp16 RNA cap 2′-O-MTase activity by site-directed mutagenesis (Lugari et al., 2010). In this study we mapped the linear domain consisting of aa 65–107 of nsp10 as the core area for the interaction with nsp16, which is located inside the interface of the nsp10/nsp16 complex as revealed from the crystal structure (Chen et al., 2011; Decroly et al., 2011). The biochemical assays between truncated proteins of nsp10 and full-length nsp16 showed that the core 2′-O-MTase activation domain of nsp10 was aa 42–120, which is overlapping with but larger than the domain for interaction with nsp16. Based on the interaction domain sequence of nsp10, we identified two short peptides which could significantly inhibit the 2′-O-MTase activity of nsp16/nsp10 complex. These peptides could be potentially developed into specific drug candidates against coronavirus.

2. Materials and methods

2.1. Construction of plasmids

The primers for nsp10 and nsp16 were designed according to the genomic sequence of SARS-CoV strain WHU (GenBank accession number: AY394850) and the templates of PCR were the cDNA of the SARS-CoV WHU strain (Pan et al., 2008). The coding sequence of SARS-CoV nsp16 was cloned into the yeast expression vector pGBKT7 (Clontech), fusing with the GAL4 DNA-binding domain, resulting in plasmid pBD16. The cDNAs of full-length and truncated nsp10 of SARS-CoV were cloned into the yeast expression vector pGADT7 (Clontech), fusing with the GAL4 activation domain, giving rise to plasmids pAD10 (aa 1–139), pAD10ΔN41 (aa 42–139), pAD10ΔN64 (aa 65–139), pAD10ΔN90 (aa 91–139), pAD10ΔC19 (aa 1–120), pAD10ΔC32 (aa 1–107), pAD10ΔC53 (aa 1–86), pAD10ΔN55&ΔC32 (aa 56–107) and pAD10ΔN64&ΔC32 (aa 65–107), respectively (Fig. 1B). For protein expression of SARS-CoV nsp16, nsp10 and its truncation mutants (nsp10ΔN41, nsp10ΔN64, nsp10ΔC19, nsp10ΔC32), the corresponding sequenceses were amplified from yeast expression plasmids by PCR and cloned into the protein expression vector pET30a(+) (Novagen). All of the clones were confirmed by DNA sequencing.

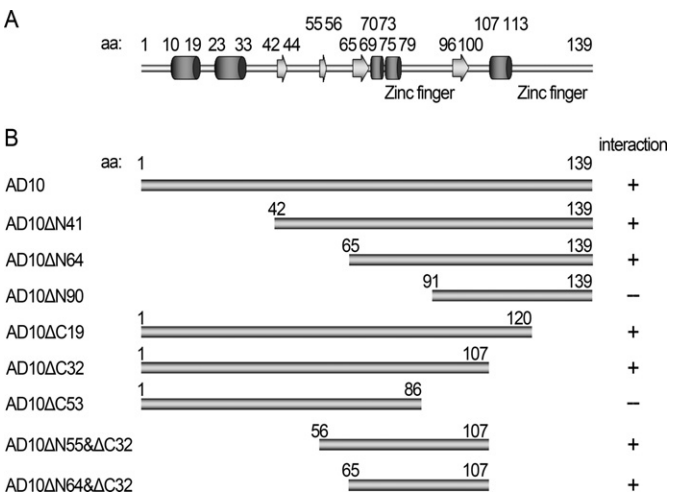

Fig. 1. Mapping of the domain of SARS-CoV nsp10 involved in the interaction with nsp16. (A) The secondary structure of nsp10 based on its crystal structure (PDB entry: 2FYG). Cylinder: alpha helix; arrow: beta sheet. (B) Summary of the interactions between nsp16 and nsp10 or its truncation mutants. The results of Y2H are shown at the right: (+) indicates positive interaction; (−) indicates negative interaction.

2.2. Yeast two-hybrid assays

Yeast strain AH109 was used to co-transform BD16 and AD10 or its truncation mutants. The transformation of yeast cells was conducted according to the manufacturer's protocol (Clontech PT3247-1). The co-transformed yeast cells were inoculated on the QDO (SD/-Ade/-His/-Trp/-Leu) screening plates at 30 °C and then performed with β-galactosidase assay according to the protocol (Clontech PT3247-1).

2.3. Expression and purification of recombinant proteins

For all recombinant protein expression plasmids, transformed *E. coli* BL21 (DE3) cells were grown at 37 °C in Luria–Bertani (LB) broth with 50 μg ml^{-1} kanamycin and induced with 0.4 mM isopropyl β-D-thiogalactopyranoside (IPTG) at 16 °C for 12–16 h. Then the cells were collected by centrifugation and resuspended in buffer A [50 mM Tris–HCl, pH 7.5, 150 mM NaCl, 5 mM $MgSO_4$, 5% glycerol] supplemented with 10 mM imidazole. After sonication and centrifugation, cleared lysates were applied to nickel–nitrilotriacetic acid (Ni–NTA) resin (Genesript) and washed with buffer A supplemented with an imidazole gradient of 20 mM, 50 mM, and 80 mM. Protein was eluted with buffer A supplemented with 250 mM imidazole. At last, the elution buffer was changed to reaction buffer [50 mM Tris–HCl, pH 7.5, 50 mM NaCl, 2 mM DTT, 10% glycerol] and fractions were frozen at −80 °C. The expression and purification of SARS-CoV nsp14 and other proteins are described previously (Chen et al., 2009).

2.4. Preparation of capped RNA substrates

RNA substrates representing the 5′-terminal 259 nucleotides of the SARS-CoV genome were in vitro transcribed, ^{32}P-labeled at cap structures (m7G*pppA-RNA or G*pppA-RNA, where the * indicates that the following phosphate was ^{32}P labeled), and purified as described previously (Chen et al., 2009, 2011). RNAs containing ^{32}P-labeled cap-1 structure (m7G*pppAm-RNA) as positive control were converted from cap-0 structure m7G*pppA-RNA by a vaccinia virus 2′-O-methyltransferase VP39 by following the manufacturer's protocol (Epicentre). RNAs containing unlabeled cap structures (m7GpppA-RNA) were in vitro transcribed and prepared

Table 1
Short peptides derived from nsp10 of SARS-CoV.

Peptide	Amino acid sequences	Position in nsp10 (aa number)
K8	PTTCANDP	100–107
K10	DLKGKYVQIP	91–100
K12	GGASCCLYCRCH	69–80
K20	NCVKMLCTHTGTGQAITVTP	40–59
K29	FGGASCCLYCRCHIDHPNPKGFCDLKGKY	68–96

as the ^{32}P-labeled cap structure RNAs except cold GTPs were used instead of ^{32}P-labeled GTPs. All the RNA substrates were extracted with phenol–chloroform and precipitated with ethanol.

2.5. Biochemical assays for MTase activity

Purified recombinant or truncated proteins (final concentration: 0.5 μM for nsp14 and nsp16, 2.6 μM for nsp10 and its truncations) and 2×10^3 cpm of ^{32}P-labeled m7G*pppA-RNA or G*pppA-RNA substrates were added to 8.5 μl reaction mixture [40 mM Tris–HCl (pH 7.5 or 8.0), 2 mM $MgCl_2$, 2 mM DTT, 10 units RNase inhibitor, 0.2 mM SAM] and incubated at 37 °C for 1.5 h. RNA cap structures were liberated with 5 μg of nuclease P1 (Sigma), then spotted onto polyethyleneimine cellulose-F plates (Merck) for thin layer chromatography (TLC), and developed in 0.4 M ammonium sulfate. The extent of ^{32}P-labeled cap was determined by scanning the chromatogram with a PhosphorImager as described previously (Chen et al., 2009, 2011).

MTase activity assays were carried out in 30 μl reaction mixture [40 mM Tris–HCl (pH 7.5), 2 mM $MgCl_2$, 2 mM DTT, 40 units RNase inhibitor, 0.01 mM SAM], with 1 μCi of S-adenosyl [methyl-^{3}H] methionine (67.3 Ci/mmol, 0.5 μCi/μl), purified SARS-CoV nsp16/nsp10 complex (final concentration: 3.3 μM for nsp16 and 14 μM for nsp10), short peptides with different final concentrations and 3 μg m7GpppA-RNA substrates at 37 °C for 1.5 h. ^{3}H-labeled product was isolated in small DEAE-Sephadex columns and quantitated by liquid scintillation (Ahola et al., 1997).

2.6. SAM binding assays

25 μl reaction mixtures [40 mM Tris–HCl (pH 7.5), 2 mM $MgCl_2$, 2 mM DTT] containing 0.5 μM purified nsp16, different concentrations of nsp10 or its truncations and 2 μCi of *S*-adenosyl [methyl-^{3}H] methionine (67.3 Ci/mmol, 0.5 μCi/μl) were pipetted into wells of a microtiter plate. The reaction mixtures were incubated on ice and irradiated with 254-nm UV light in a Hoefer UVC500 cross-linking oven for 30 min. The distance of samples from the UV tubes was 4 cm. The samples were then analyzed by 12% sodium dodecyl sulfate-polyacrylamide gel electrophoresis (SDS-PAGE). The gels were socked in Enlightening buffer (PerkinElmer) and analyzed by autoradiography (Ahola et al., 1997)

2.7. Structural modeling and peptide synthesis

Structure data used in this study were from PDB entry 2FYG and PDB entry 3R24 (Chen et al., 2011; Joseph et al., 2006). Based on the crystal structure and our previous analysis, five short peptides named K8, K10, K12, K20 and K29 were designed and then synthesized (Shanghai Ji'er Biochemistry)with N-terminal acetylated and C-terminal amidated modifications (Table 1). Peptides were purified to >95% purity by HPLC and verified by mass spectrometry. Peptide K12 was first dissolved in DMSO and further diluted in water and the maximum final concentration of DMSO in peptide K12 was 0.12%. The other four peptides were dissolved in distilled water directly.

3. Results

3.1. Mapping of the SARS-CoV nsp10 domain involved in the interaction with nsp16

We assume that the minimal domain of nsp10 that is essential for association with nsp16 should be smaller than the region observed in the nsp10/nsp16 complex. Thus, we initiated to map the minimal interaction domain of nsp10 by adopting the yeast two-hybrid system, which was well established for studying the interactions between nsp10 and nsp16 (Imbert et al., 2008; Pan et al., 2008). As SARS-CoV nsp10 possesses transcriptional activation activity, which activated reporter gene when fused with DNA-binding domain (data not shown), nsp16 was cloned into the DNA-binding domain vector while all the nsp10 truncation mutants were cloned into activation domain vector. Based on the crystal structure of nsp10 (PDB entry: 2FYG and 3R24) (Chen et al., 2011; Joseph et al., 2006), we designed and cloned eight plasmids to express truncated proteins in yeast two-hybrid system (Fig. 1A). As shown in Fig. 1B, the truncation mutants of nsp10 AD10ΔN41 (ΔN41 indicates the truncation of N-terminal 41 amino acids in SARS-CoV nsp10, and other mutants are named in similar manner) and AD10ΔN64 could still maintain the interaction with nsp16, but when the N-terminal 90 aa (AD10ΔN90) were deleted, the interaction with nsp16 was abolished, suggesting that the first 64 aa at the N-terminus is dispensable for the interaction. And when the C-terminal 19 and 32 aa (AD10ΔC19 and AD10ΔC32) were truncated, there were no influences on the interaction until C-terminal 53 aa (AD10ΔC53) were removed, indicating that the C-terminal 32 aa of nsp10 were not needed for the interaction with nsp16. Taken together, the shortest region of nsp10 essential for its interaction with nsp16 identified in above assays was aa 65–107 in nsp10 (Fig. 1B). The minimal interaction domain of nsp10 represents part of the interaction surface and can be clearly recognized in the crystal structure of nsp10/nsp16 complex (Chen et al., 2011; Decroly et al., 2011).

3.2. Identification of the region of aa 42–120 of nsp10 as the functional domain for activating nsp16 in vitro

Although the interaction domain essential for interaction with nsp16 was identified, it is still not known which region of nsp10 is sufficient to stimulate the nsp16 2′-O-MTase activity. To determine the stimulatory domain of nsp10, we expressed and purified full-length nsp10 and four truncated derivatives in addition to full-length nsp14 and nsp16 (Fig. 2A and B). The methodology for analyzing the 2′-O-MTase activity of nsp10/nsp16 complex was established in our previous work (Chen et al., 2011). As shown in Fig. 2C, by using radiolabeled and unmethylated G*pppA-capped RNA as substrate (where the * indicates that the following phosphate was ^{32}P labeled, and the sequence is identical with viral genomic RNA except for the second nucleotide changed from U to G), we confirmed that nsp10/nsp14/nsp16 could methylate G*pppA-RNA to m7G*pppAm-RNA (Fig. 2C, lane 2), in which nsp14 methylates G*pppA-RNA at N7 position of guanine (m7G) to generate cap-0 m7GpppA-RNA first (Fig. 2C, lanes 1 and 7), followed by the methylation of m7G*pppA-RNA at the 2′-O-position of adenine (Am) to generate cap-1 m7G*pppAm-RNA. Two truncation mutants nsp10ΔC19 (by removal of C-terminal 19 aa) and nsp10ΔN41 (by removal of N-terminal 41 aa) could activate nsp16 MTase activity as effectively as full-length nsp10 when mixed with nsp14/nsp16 (Fig. 2C, lanes 5 and 6). However, truncation mutants nsp10ΔC32 (by removal of C-terminal 32 aa) and nsp10ΔN64 (by removal of N-terminal 64 aa) lost the stimulation activity to activate the nsp16 2′-O-MTase (Fig. 2C, lanes 3 and 4). These results indicated that the region of aa 42–120 of nsp10 was involved in the

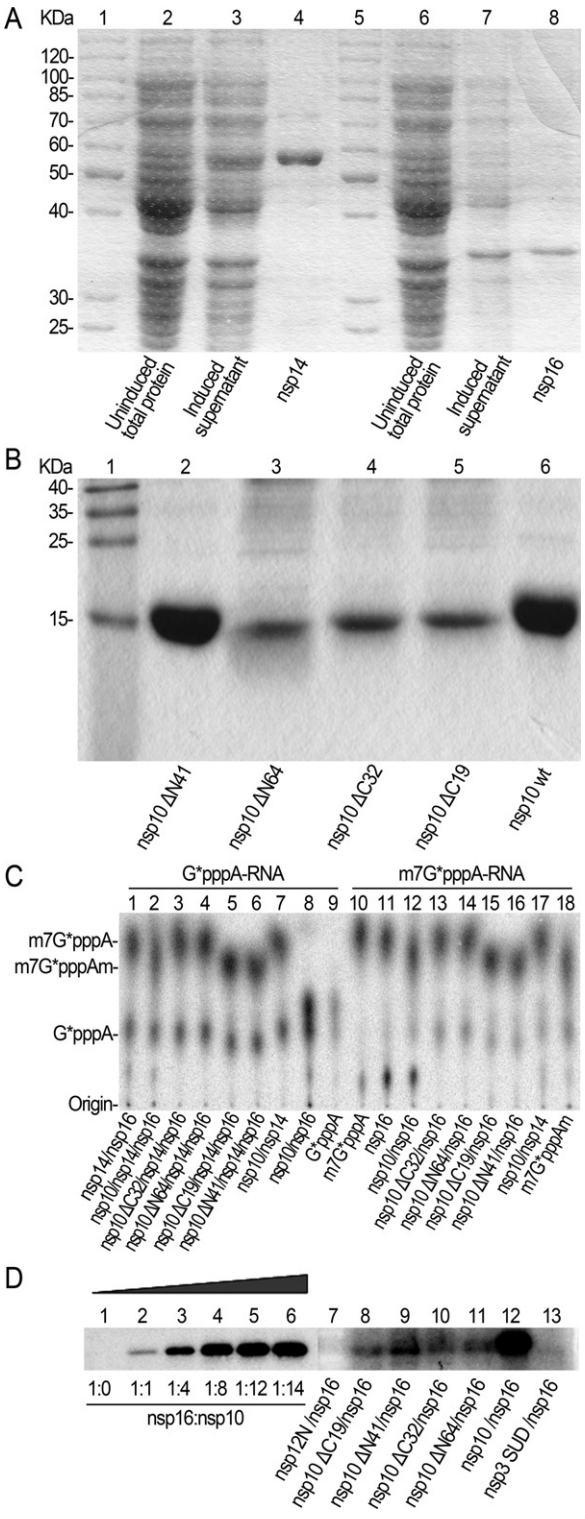

Fig. 2. Biochemical analyses of SARS-CoV nsp10 and its truncation mutants in stimulating MTase activity and SAM binding of nsp16. (A) Purification and SDS-PAGE analysis of recombinant nsp14 (lane 4) and nsp16 (lane 8). The sizes of protein markers (lanes 1 and 5) are indicated on the left. (B) Purification and SDS-PAGE analysis of recombinant nsp10 (lane 6) and its truncation mutants: nsp10ΔN41 (lane 2); nsp10ΔN64 (lane 3); nsp10ΔC32 (lane 4) and nsp10ΔC19 (lane 5). The sizes of protein markers (lane 1) are indicated on the left. (C) TLC analysis of nuclease P1-resistant cap structures released from ^{32}P-labeled G*pppA-RNA (lanes 1–9) and m7G*pppA-RNA (lanes 10–18) methylated by different protein combinations, respectively. The positions of origin and migration of G*pppA, m7G*pppA, m7G*pppAm (lanes 8, 9 and 18) are indicated on the left. (D) SAM binding analyses of nsp16 supplemented with nsp10 or its truncation mutants. The SAM binding assays were performed at different ratios of nsp10/16 (lanes 1–6) or treated with different protein combinations: nsp12N/nsp16, nsp10ΔC19/nsp16, nsp10ΔN41/nsp16, nsp10ΔC32/nsp16, nsp10ΔN64/nsp16, nsp10/nsp16, nsp3SUD/nsp16, respectively (lanes 7–13).

stimulation of nsp16 MTase activity and it is overlapping in part with but larger than the interaction domain identified above. Such data implied that the aa 42–64 and aa 108–120 of nsp10, which flanks the interaction domain, are essential for stimulation of nsp16 but not essential for the association with nsp16. When the substrate m7G*pppA-RNA (which was first N7-methylated by nsp14) were used, we obtained the same results (Fig. 2C, lanes 13–16). Collectively, aa 42–120 of nsp10 was identified as the functional domain of SARS-CoV nsp10 to stimulate nsp16 MTase activity.

S-adenosyl-methionine (SAM) is the substrate of methyltransferase, and one function of nsp10 involved in the stimulation of nsp16 enzymatic activity is to promote the SAM-binding activity of nsp16 (Chen et al., 2011). Therefore, we tested whether the loss of stimulating activity of nsp10 mutants correlated with the defect of SAM-binding of nsp16. Although the 1:1 ratio of nsp10 to nsp16 was observed in the crystal structure of nsp10/nsp16 complex (Chen et al., 2011; Decroly et al., 2011), we found that the higher the molar ratio of nsp10 to nsp16 in the reaction mixture, the higher the SAM-binding affinity of nsp16 (Fig. 2D, lanes 1–6). The influence of nsp10 truncation on the SAM binding affinity of nsp16 was tested at the molar ratio 8:1 of nsp10 or mutants to nsp16. As shown in Fig. 2D, all four truncated proteins attenuated the SAM binding affinity of nsp16 (Fig. 2D, lanes 8–11) in comparison with wild-type nsp10 (Fig. 2D, lane 12). The SAM-binding affinity of nsp16 in complex with nsp10ΔC19 and nsp10ΔN41 (Fig. 2D, lanes 8 and 9) was higher than that with nsp10ΔC32 and nsp10ΔN64 (Fig. 2D, lanes 10 and 11). However, the 2′-O-MTase activity of nsp16 mixed with nsp10ΔC32 and nsp10ΔN64 was completely abolished (Fig. 2C, lanes 3, 4, 13 and 14), indicating that these two truncation mutants were also defective in some process other than SAM-binding. Altogether, these data suggest that aa 42–64 and aa 108–120 of nsp10, which flank the nsp10 core interaction domain, play an important role in stimulating the MTase activity of nsp16, and the integrity of nsp10 was needed to fully stimulate the SAM-binding activity of nsp16.

3.3. Design and analysis of peptides that partially mimic the interaction domain of nsp10 for inhibition of nsp16 MTase activity

As described above, the interaction domain of nsp10 (aa 65–107, indicated in blue in Fig. 3A and B) is one part of the functional domain (aa 42–120) that could stimulate the 2′-O-MTase activity of nsp16, the latter also consisting of aa 42–64 (red in Fig. 3A and B) and aa 108–120 in nsp10 (pink in Fig. 3A and B). Due to the difference of the interaction domain and the functional stimulatory domain of nsp10, we presumed that peptides representing part of the interaction or stimulatory domain of nsp10 might be able to inhibit the 2′-O′-MTase activity of nsp16 by interfering with the association of nsp10 and nsp16 or preventing from correct assembly of nsp10/nsp16 complex. Based on previous mutational analysis of nsp10 and the crystal structure of nsp10/nsp16 complex, we designed and chemically synthesized five peptides that mimic part of the stimulatory or interaction domain without destroying the secondary structure of nsp10: K20 (aa 40–59), K29 (aa 68–96), K12 (aa 68–80), K10 (aa 91–100) and K8 (aa 100–107) (Fig. 3C). The choice of this particular set of peptides was mainly based on the consideration to keep the peptides short (less than 30 aa) and stable in secondary structure.

To evaluate the inhibitory effect of synthesized peptides on 2′-O-MTase of nsp16, the peptides at various concentrations were added to the mixture of nsp16 (final concentration 3.3 μM) and nsp10

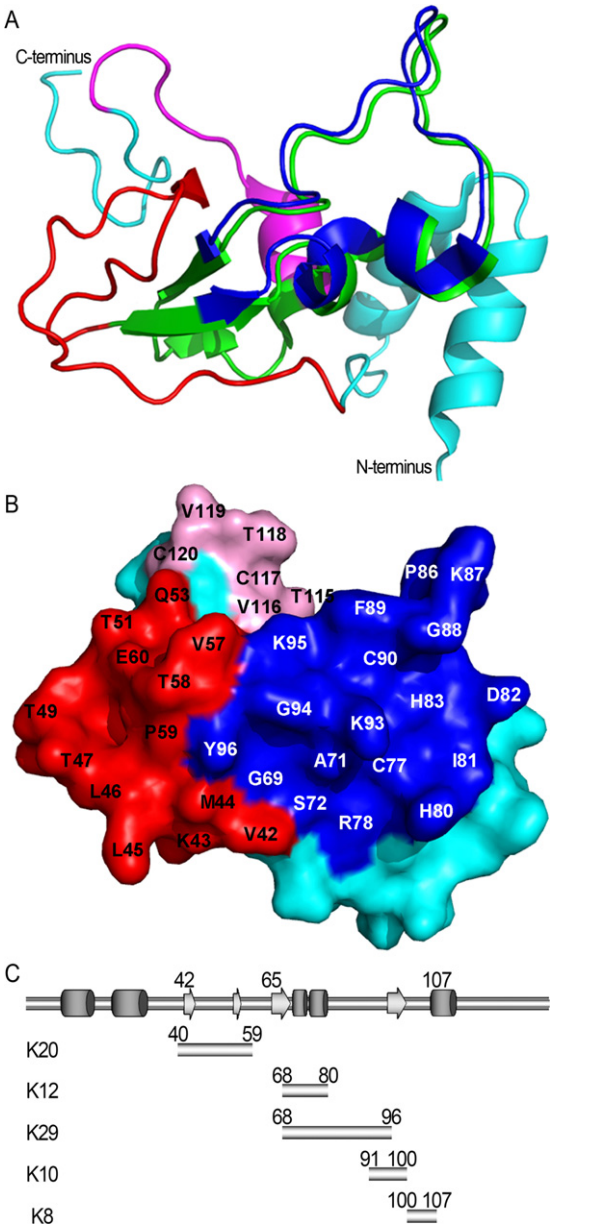

Fig. 3. Position of the interaction and functional domains of nsp10 and the short peptides located in nsp10. (A) The location of the peptide segments of SARS-CoV nsp10 is shown in ribbon structure: green for core interaction domain (aa 65–107), both red (aa 42–64) and pink (108–120) as essential regions for stimulating nsp16, cyan for non-essential parts for both interaction and stimulation (aa 1–42 and aa 120–139). The peptide K29 (aa 68–96, in blue) is superimposed with nsp10. (B) The surface view of (A). The core interaction domain is in blue. The positions of amino acids are marked on the surface of nsp10. (C) Summary of short peptides corresponding to the region of nsp10.

(final concentration 14 μM) in the MTase activity assays, in which ^{3}H-labeled SAM was used as a methyl group donor. As shown in Fig. 4A, K29 and K12 could markedly inhibit the activity of nsp16 in a dose-dependent manner, and the inhibitory concentration of 50% was approximately 160 μM for both two peptides. In contrast, K8, K10 and K20 could not efficiently suppress the enzymatic activity of nsp16 even at the concentration of 320 μM. Therefore, these results showed that peptides K12 and K29 could significantly inhibit 2′-O-MTase activity of nsp16.

We then checked whether the inhibition of the peptides on the 2′-O-MTase activity was due to the attenuation of SAM-binding activity of nsp16 (Fig. 4B). As shown in Fig. 4B, when the molar ratio

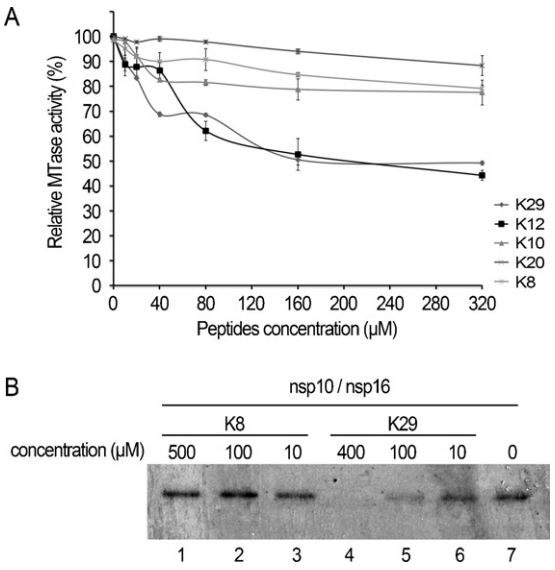

Fig. 4. Inhibitory effect and interference with SAM binding of nsp10/nsp16 complex by short peptides. (A) Inhibition effect of short peptides at different concentrations (n = 3, mean values ± SD). (B) SAM binding analyses of SARS-CoV nsp10 and nsp16 at different concentrations of short peptides K8 (lanes 1–3) and K29 (lanes 4–6). The concentrations of the peptides are indicated above the autographic image. The positive control without any peptide added is shown in lane 7.

of nsp16/nsp10 complex was 8:1, K29 decreased the SAM binding by nsp16 in a dose-dependent manner. When 400 μM of K29 was used, it almost abolished the SAM-binding activity of nsp16 (Fig. 4B, lane 4). In contrast, the peptide K8, which could not inhibit the 2′-O-MTase activity, had no effect on SAM binding of nsp16, even when the final concentration of 500 μM was applied (Fig. 4B, lanes 1–3). In conclusion, the peptides that inhibited enzymatic activity interfered with the SAM-binding activity of nsp16.

4. Discussion

The association between SARS-CoV nsp10 and nsp16 and the stimulatory effect of nsp10 on nsp16 2′-O-MTase activity was revealed previously (Bouvet et al., 2010; Chen et al., 2011; Imbert et al., 2008; Pan et al., 2008). In this study, we showed that the area aa 65–107 in nsp10 was sufficient for its interaction with nsp16 while the domain of aa 42–120 in nsp10 is the essential region for nsp16 to complete its enzymatic activity, which indicates that the interaction and functional stimulatory domains are overlapping but different in length. Furthermore, we identified two peptides (K12 and K29), which were derived from the interaction domain of nsp10 and could significantly inhibit the 2′-O-MTase activity of SARS-CoV nsp10/16 complex.

The interaction between nsp10 and nsp16 was identified originally by using yeast and mammalian two-hybrid systems in our and others' previous work (Imbert et al., 2008; Pan et al., 2008), and the interaction domain of nsp10 identified by a yeast two-hybrid system in this study could be recognized from the crystal structure revealed recently (Chen et al., 2011; Decroly et al., 2011), suggesting that the feasibility to use the yeast two-hybrid system for mapping the interaction domain of nsp10. The structural data show that significant contact between nsp10 and nsp16 exists and it involves aa 40–47/69–84/93–96 of nsp10 or 40–47/57–59/69–72/77–84/93–96 of nsp10 as shown previously (Chen et al., 2011; Decroly et al., 2011). Lugari and colleagues reported that several 'hot spots' such as V42, M44, A71, K93, G94 and Y96 form a continuous protein-protein surface within a central core of nsp10 (Fig. 3B) and are important for the stimulatory effect

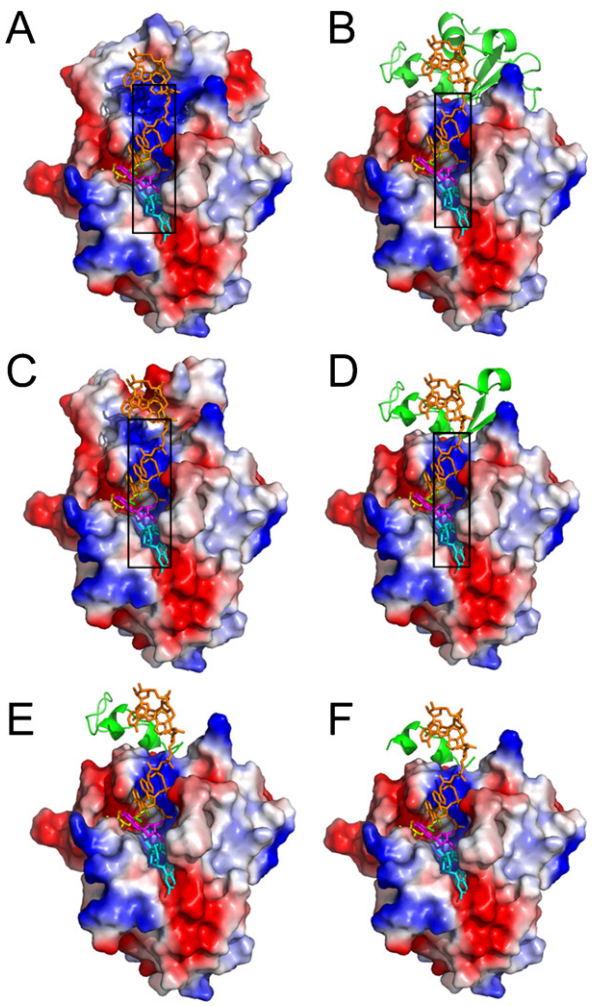

Fig. 5. Overall structure of nsp16 docked with nsp10 truncation mutants. The stimulatory domain (aa 42–120) of nsp10 (A and B), the interaction domain (aa 65–107) of nsp10 (C and D), the peptides K29 (aa 68–96) (E) and K12 (aa 68–80) (F) are docked with nsp16, respectively. Nsp16 is shown as electrostatic potential surface (positive charged surface is colored in blue, negative charged surface is colored in red). The portions of nsp10 domains and peptides (K29 and K12) are shown as electrostatic potential surface with 20% transparency (A and C) and ribbon (B, D–F), respectively. The methyl donor SAM (colored in yellow) and the capped RNA substrate m7GpppA-RNA (cap structure m7Gppp- is colored in cyan, the first nucleotide A is colored in magenta, and the rest nucleotides of RNA substrate are colored in orange) are docked into the complex. The RNA binding groove is indicated by black box.

of nsp10 (Lugari et al., 2010), which is consistent with the analysis of the crystal structure. Interestingly, in this study, we revealed that not all the area that is in contact with nsp16 observed in the crystal structure is needed for its stable association with nsp16. For example, the stretch of aa 40–47 was dispensable for the interaction but needed for its stimulatory function on nsp16 MTase activity.

The mechanism for nsp10 to stimulate nsp16 is to promote its SAM binding and to stabilize its RNA binding capacity of nsp16 (Chen et al., 2011). Therefore, the mechanism for peptide inhibition may be their interference with the SAM binding and/or RNA binding capacity of nsp16. According to the docking model of nsp16/nsp10 complex with m7GpppA-RNA, the areas of nsp10 that help nsp16 to stabilize RNA binding are mainly aa 9–13 and 39–41 (Chen et al., 2011). In this study we have shown that the functional area of nsp10 for stimulating nsp16 is the region of aa 42–120, which means that aa 1–41 of nsp10 is dispensable for nsp16 stimulation. When the stimulatory domain (aa 42–120) of nsp10 is docked with nsp16 (Fig. 5A and B), the RNA-binding groove (depicted in blue in Fig. 5A) is similarly extended as with full-length nsp10 (Chen et al., 2011), and this may explain why the region of aa 42–120 of nsp10 could stimulate nsp16 as efficiently as full-length nsp10.

All of the four truncation mutants of nsp10, nsp10ΔC32 (aa 1–107), nsp10ΔC19 (aa 1–120), nsp10ΔN64 (aa 65–139) and nsp10ΔN41 (aa 42–139), decreased the capacity of SAM-binding of nsp16 in the biochemical assays (Fig. 2D), which indicates that the integrity of nsp10 is important for reaching full enzymatic activity of nsp16. The monomer structure of nsp10 is identical to that in complex with nsp16, but the monomer structure of nsp16 has not been resolved (Chen et al., 2011). It is conceivable that conformational changes of nsp16 may take place after binding with nsp10 and such changes may play a role in activating the MTase activity of nsp16 because the monomeric nsp16 of SARS-CoV could not show any MTase activity until in complex with nsp10. Therefore, one possible explanation for the inhibition seen with the peptides may be due to the effects on nsp16 conformational changes.

There are 2 α-helices, 2 β-sheets and a Zn-finger motif in the interaction area of nsp10 (aa 65–107) (Fig. 3A), which indicates this area could form rigid structure. Such assumption is consistent with the observation that nsp10 structure is not changed when in association with nsp16 (Chen et al., 2011; Decroly et al., 2011). However, the area of aa 42–64 consists of flexible loops which are in vicinity of the interaction surface and this part may take part in the functional regulation or induce conformational changes of nsp16 (Fig. 5). In addition, there is an α-helix in the functional area of aa 108–120 of nsp10, which is positively charged and stays away from the interaction domain, and thus we assume that the function of this part may be its involvement in stabilizing the SAM-binding pocket and/or RNA-binding groove of nsp16 (Fig. 5A and B). When just the interaction domain (aa 65–107) is docked with nsp16 (Fig. 5C and D), the RNA-binding groove (in blue) of nsp16 is not extended significantly. This may partially explain why the interaction domain (aa 65–107) of nsp10 is sufficient for interaction with nsp16 but deficient in activating nsp16 enzymatic activity. Such observation provides the rationale for designing short peptides, which represent part of the interaction domain of nsp10, for inhibiting the enzymatic activity of nsp10/16 complex. In this study, two short peptides (K29 and K12) showed inhibitory effects on the enzymatic activity of nsp10/16 (Fig. 4A) and their relative location is shown in the structural models (Fig. 5E, and F). The inhibition of the two peptides on the 2′-O-MTase activity of nsp10/nsp16 was relatively weak but the structural information may help to develop more effective small molecule inhibitors or modified peptides (including cyclic peptides). The inhibitory effect of the peptides may result from their competition with nsp10 for binding nsp16 and/or their interference with the formation of correct conformation of nsp10/16 complex. When peptides K29 and K12 were added to nsp16 in absence of nsp10, the association of the peptides with nsp16 could not be demonstrated in the isothermal titration calorimetric assays (data not shown), and this observation suggested that the inhibitory effect of the peptides may be mainly due to their interference with formation of correct conformation of nsp10/16 complex.

It has been nine years since the outbreak of SARS in 2003, however there is still no effective drug for control of coronaviruses including SARS-CoV. There are three types of antivirals developed for SARS-CoV: (1) virus entry blockers, such as monoclonal antibodies to spike protein, peptides that bind to the heptad repeat on the spike protein, and peptides that bind to other regions of the spike and block its oligomerization; (2) virus replication blockers, such as protease inhibitors, viral polymerase inhibitors, small interfering RNAs and ribavirin; (3) immune modulators, such as type I interferon, and ritonavir (Anderson and Tong, 2010; Groneberg et al., 2005; Tong, 2009a,b). In addition, some small molecules are reported to inhibit the MTase activity of nsp16, such as SAH (S-adenosyl-l-homocysteine), sinefungin and ATA (Bouvet et al., 2010; Decroly et al., 2011; He et al., 2004). Here we report two peptides

(K12 and K29) that could inhibit the 2′-O-methlytranferase activity of nsp16 by decreasing its SAM-binding activity. As far as we know, they are the first peptides designed to inhibit cap modification enzymes of any viruses.

In conclusion, we identified the interaction domain and the functional region of nsp10 that stimulates the 2′-O-MTase activity of nsp16. The results provide more insights into the mechanism of coronavirus capping and RNA methylation. We also designed and synthesized two inhibitory peptides K12 and K29 that could inhibit the MTase activity of nsp10/nsp16 complex, and such peptides may be further developed into potential specific antivirals against coronavirus infection.

Acknowledgments

This study was supported by China Basic Research Program (#2010CB911800) and China NSFC grants (#30925003, #81130083, #30921001 and #31000085).

References

Ahola, T., Laakkonen, P., Vihinen, H., Kaariainen, L., 1997. Critical residues of Semliki Forest virus RNA capping enzyme involved in methyltransferase and guanylyltransferase-like activities. Journal of Virology 71 (1), 392–397.

Anderson, L.J., Tong, S., 2010. Update on SARS research and other possibly zoonotic coronaviruses. International Journal of Antimicrobial Agents 36 (Suppl. 1), S21–S25.

Bouvet, M., Debarnot, C., Imbert, I., Selisko, B., Snijder, E.J., Canard, B., Decroly, E., 2010. In vitro reconstitution of SARS-coronavirus mRNA cap methylation. PLoS Pathogens 6 (4), e1000863.

Chen, P., Jiang, M., Hu, T., Liu, Q., Chen, X.S., Guo, D., 2007. Biochemical characterization of exoribonuclease encoded by SARS coronavirus. Journal of Biochemistry and Molecular Biology 40 (5), 649–655.

Chen, Y., Cai, H., Pan, J., Xiang, N., Tien, P., Ahola, T., Guo, D., 2009. Functional screen reveals SARS coronavirus nonstructural protein nsp14 as a novel cap N7 methyltransferase. Proceedings of the National Academy of Sciences of the United States of America 106 (9), 3484–3489.

Chen, Y., Su, C., Ke, M., Jin, X., Xu, L., Zhang, Z., Wu, A., Sun, Y., Yang, Z., Tien, P., Ahola, T., Liang, Y., Liu, X., Guo, D., 2011. Biochemical and structural insights into the mechanisms of SARS coronavirus RNA ribose 2′-O-methylation by nsp16/nsp10 protein complex. PLoS Pathogens 7 (10), e1002294.

Daffis, S., Szretter, K.J., Schriewer, J., Li, J., Youn, S., Errett, J., Lin, T.Y., Schneller, S., Zust, R., Dong, H., Thiel, V., Sen, G.C., Fensterl, V., Klimstra, W.B., Pierson, T.C., Buller, R.M., Gale Jr., M., Shi, P.Y., Diamond, M.S., 2010. 2′-O-methylation of the viral mRNA cap evades host restriction by IFIT family members. Nature 468 (7322), 452–456.

Debarnot, C., Imbert, I., Ferron, F., Gluais, L., Varlet, I., Papageorgiou, N., Bouvet, M., Lescar, J., Decroly, E., Canard, B., 2011. Crystallization and diffraction analysis of the SARS coronavirus nsp10–nsp16 complex. Acta Crystallographica. Section F, Structural Biology and Crystallization Communications 67 (Pt 3), 404–408.

Decroly, E., Debarnot, C., Ferron, F., Bouvet, M., Coutard, B., Imbert, I., Gluais, L., Papageorgiou, N., Sharff, A., Bricogne, G., Ortiz-Lombardia, M., Lescar, J., Canard, B., 2011. Crystal structure and functional analysis of the SARS-coronavirus RNA cap 2′-O-methyltransferase nsp10/nsp16 complex. PLoS Pathogens 7 (5), e1002059.

Decroly, E., Imbert, I., Coutard, B., Bouvet, M., Selisko, B., Alvarez, K., Gorbalenya, A.E., Snijder, E.J., Canard, B., 2008. Coronavirus nonstructural protein 16 is a cap-0 binding enzyme possessing (nucleoside-2′O)-methyltransferase activity. Journal of Virology 82 (16), 8071–8084.

Dong, H., Zhang, B., Shi, P.Y., 2008. Flavivirus methyltransferase: a novel antiviral target. Antiviral Research 80 (1), 1–10.

Dos Ramos, F., Carrasco, M., Doyle, T., Brierley, I., 2004. Programmed-1 ribosomal frameshifting in the SARS coronavirus. Biochemical Society Transactions 32 (Pt 6), 1081–1083.

Groneberg, D.A., Poutanen, S.M., Low, D.E., Lode, H., Welte, T., Zabel, P., 2005. Treatment and vaccines for severe acute respiratory syndrome. Lancet Infectious Diseases 5 (3), 147–155.

He, R., Adonov, A., Traykova-Adonova, M., Cao, J., Cutts, T., Grudesky, E., Deschambaul, Y., Berry, J., Drebot, M., Li, X., 2004. Potent and selective inhibition of SARS coronavirus replication by aurintricarboxylic acid. Biochemical and Biophysical Research Communications 320 (4), 1199–1203.

Imbert, I., Snijder, E.J., Dimitrova, M., Guillemot, J.C., Lecine, P., Canard, B., 2008. The SARS-coronavirus PLnc domain of nsp3 as a replication/transcription scaffolding protein. Virus Research 133 (2), 136–148.

Joseph, J.S., Saikatendu, K.S., Subramanian, V., Neuman, B.W., Brooun, A., Griffith, M., Moy, K., Yadav, M.K., Velasquez, J., Buchmeier, M.J., Stevens, R.C., Kuhn, P., 2006. Crystal structure of nonstructural protein 10 from the severe acute respiratory syndrome coronavirus reveals a novel fold with two zinc-binding motifs. Journal of Virology 80 (16), 7894–7901.

Lugari, A., Betzi, S., Decroly, E., Bonnaud, E., Hermant, A., Guillemot, J.C., Debarnot, C., Borg, J.P., Bouvet, M., Canard, B., Morelli, X., Lecine, P., 2010. Molecular mapping of the RNA Cap 2′-O-methyltransferase activation interface between severe acute respiratory syndrome coronavirus nsp10 and nsp16. Journal of Biological Chemistry 285 (43), 33230–33241.

Minskaia, E., Hertzig, T., Gorbalenya, A.E., Campanacci, V., Cambillau, C., Canard, B., Ziebuhr, J., 2006. Discovery of an RNA virus 3′->5′ exoribonuclease that is critically involved in coronavirus RNA synthesis. Proceedings of the National Academy of Sciences of the United States of America 103 (13), 5108–5113.

Moheshwarnath Issur, F.d.r.P.-J.a.M.B., 2011. The RNA capping machinery as an anti-infective target. In: WIREs RNA, vol. 2, pp. 184–192, doi:10.1002/wrna.43.

Pan, J., Peng, X., Gao, Y., Li, Z., Lu, X., Chen, Y., Ishaq, M., Liu, D., Dediego, M.L., Enjuanes, L., Guo, D., 2008. Genome-wide analysis of protein–protein interactions and involvement of viral proteins in SARS-CoV replication. PLoS One 3 (10), e3299.

Shuman, S., 2001. The mRNA capping apparatus as drug target and guide to eukaryotic phylogeny. Cold Spring Harbor Symposia on Quantitative Biology 66, 301–312.

Snijder, E.J., Bredenbeek, P.J., Dobbe, J.C., Thiel, V., Ziebuhr, J., Poon, L.L., Guan, Y., Rozanov, M., Spaan, W.J., Gorbalenya, A.E., 2003. Unique and conserved features of genome and proteome of SARS-coronavirus, an early split-off from the coronavirus group 2 lineage. Journal of Molecular Biology 331 (5), 991–1004.

Su, D., Lou, Z., Sun, F., Zhai, Y., Yang, H., Zhang, R., Joachimiak, A., Zhang, X.C., Bartlam, M., Rao, Z., 2006. Dodecamer structure of severe acute respiratory syndrome coronavirus nonstructural protein nsp10. Journal of Virology 80 (16), 7902–7908.

Tong, T.R., 2009a. Therapies for coronaviruses. Part 2: Inhibitors of intracellular life cycle. Expert Opinion on Therapeutic Targets 19 (4), 415–431.

Tong, T.R., 2009b. Therapies for coronaviruses Part I of II—viral entry inhibitors. Expert Opinion on Therapeutic Targets 19 (3), 357–367.

van Hemert, M.J., van den Worm, S.H., Knoops, K., Mommaas, A.M., Gorbalenya, A.E., Snijder, E.J., 2008. SARS-coronavirus replication/transcription complexes are membrane-protected and need a host factor for activity in vitro. PLoS Pathogens 4 (5), e1000054.

von Brunn, A., Teepe, C., Simpson, J.C., Pepperkok, R., Friedel, C.C., Zimmer, R., Roberts, R., Baric, R., Haas, J., 2007. Analysis of intraviral protein–protein interactions of the SARS coronavirus ORFeome. PLoS One 2 (5), e459.

Zust, R., Cervantes-Barragan, L., Habjan, M., Maier, R., Neuman, B.W., Ziebuhr, J., Szretter, K.J., Baker, S.C., Barchet, W., Diamond, M.S., Siddell, S.G., Ludewig, B., Thiel, V., 2011. Ribose 2′-O-methylation provides a molecular signature for the distinction of self and non-self mRNA dependent on the RNA sensor Mda5. Nature Immunology 12 (2), 137–143.